HHS Public Access

Author manuscript

Cell. Author manuscript; available in PMC 2020 August 22.

Published in final edited form as:

Cell. 2019 August 22; 178(5): 1231–1244.e11. doi:10.1016/j.cell.2019.07.033.

GDF15 is an Inflammation-Induced Central Mediator of Tissue Tolerance

Harding H. Luan[1,6,8], **Andrew Wang**[1,2,8,*], **Brandon K. Hilliard**[1,2], **Fernando Carvalho**[1], **Connor E. Rosen**[1], **Amy M. Ahasic**[3], **Erica L. Herzog**[3], **Insoo Kang**[2], **Margaret A. Pisani**[3], **Shuang Yu**[1], **Cuiling Zhang**[1,2], **Aaron M. Ring**[1], **Lawrence H. Young**[4,5], **Ruslan Medzhitov**[1,7,9,*]

[1]Department of Immunobiology, Yale University School of Medicine, New Haven, CT 06520, USA.

[2]Department of Medicine (Rheumatology), Yale University School of Medicine, New Haven, CT 06520, USA.

[3]Department of Medicine (Pulmonary and Critical Care), Yale University School of Medicine, New Haven, CT 06520, USA.

[4]Department of Medicine (Cardiology), Yale University School of Medicine, New Haven, CT 06520, USA.

[5]Department of Cellular and Molecular Physiology, Yale University School of Medicine, New Haven, CT 06520, USA.

[6]Howard Hughes Medical Institute

[7]These authors contributed equally to this work

[8]Present address: NGM Biopharmaceuticals, South San Francisco, CA 94080, USA.

[9]Present address: Department of Medicine (Pulmonary and Critical Care), Norwalk Hospital, Nuvance Health, Norwalk, CT 06856, USA)

Summary

Growth and Differentiation Factor 15 (GDF15) is an inflammation-associated hormone with poorly defined biology. Here we investigated the role of GDF15 in bacterial and viral infections. We found that inflammation induced GDF15, and that GDF15 was necessary for surviving both bacterial and viral infections, as well as sepsis. The protective effects of GDF15 were largely independent of pathogen control or the magnitude of inflammatory response, suggesting a role in

*Correspondence: ruslan.medzhitov@yale.edu or andrew.wang@yale.edu.

AUTHOR CONTRIBUTIONS

H.H.L., A.W., and R.M. designed the study, analyzed the data, and wrote the manuscript with input from the other authors. H.H.L., B.K.H., and A.W. performed the experiments with help from C.Z. and S.Y. A.M.R., B.K.H., and C.E.R. produced mouse GDF15. F.C. performed iDISCO and analyses of c-FOS staining. I.K. provided samples from the Yale Lupus Registry. A.M.A., E.L.H. and M.A.P. provided samples from the Yale MICU Biorepository. L.H.Y. provided help and advice with cardiac measurements.

DECLARATION OF INTERESTS

H.H.L. is currently an employee of NGM Biopharmaceuticals. A.W. received funding from NGM Biopharmaceuticals for research projects unrelated to this study through the Yale Office of Sponsored Projects.

Data and Code Availability

This study did not generate any datasets/code amenable for depositing into public repositories.

disease tolerance. Indeed, we found that GDF15 was required for hepatic sympathetic outflow and triglyceride metabolism. Failure to defend the lower limit of plasma triglyceride levels was associated with impaired cardiac function and maintenance of body temperature, effects which could be rescued by exogenous administration of lipids. Together, we show that GDF15 coordinates tolerance to inflammatory damage through regulation of triglyceride metabolism.

Introduction

Host defense against pathogens involves two distinct strategies: resistance and tolerance. Resistance involves detection and elimination of the pathogens while tolerance is characterized by adaptation to the presence of the pathogens (Ayres and Schneider, 2012; Medzhitov et al., 2012; Raberg et al., 2007; Schafer, 1971; Soares et al., 2017). While resistance has been the primary focus of research in infection biology, emerging phenomenological and mechanistic evidence points to a critical role of tolerance in host defense. Indeed, in plants, arthropods, and vertebrates, it has been shown that genetic backgrounds can uncouple fitness of an infected organism from pathogen clearance (Ayres et al., 2008; Raberg et al., 2007; Salmon and Laude, 1932). This suggests that the ability to tolerate both damage from the pathogen and collateral damage from the immune response is an essential aspect of the host defense.

Tissue protection from inflammatory damage is the limiting factor for improving clinical outcomes in many diseases. For example, in sepsis, mortality is thought to be caused by maladaptive inflammation in response to a systemic infection (Angus and van der Poll, 2013; van der Poll et al., 2017). In many cases, the inciting pathogen can be eliminated through an ever-growing selection of antibiotics and antivirals, but inflammation and resulting tissue damage can only by managed by supportive care. A mechanistic understanding of tolerance should allow development of targeted therapeutics to better protect tissues from inflammatory damage and thereby improve survival. The same principles can be extended to other acute diseases, such as stroke and myocardial infarction, in which inflammation has been shown to be an important driver of tissue damage (Anrather and Iadecola, 2016; de Groot and Rauen, 2007; Frangogiannis, 2014).

To this end, several recent studies have made efforts to better understand mechanistic aspects of tolerance in vertebrates. Notably, all of these studies find that metabolic alterations in the setting of infection play a critical role in tolerance (Rao et al., 2017; Sanchez et al., 2018; Wang et al., 2016; Weis et al., 2017). Collectively, these findings demonstrate that metabolic changes in response to inflammation and infection are essential to tissue tolerance and motivate the identification of signaling pathways by which metabolism is controlled in inflammatory settings to facilitate tissue tolerance.

Growth and Differentiation Factor 15 (GDF15), previously known as NSAID-activated gene 1 (NAG-1) and macrophage inhibitory cytokine 1 (MIC-1), is a divergent TGF-β family member historically associated with cancer cachexia, cardiovascular disease, and a host of other diseases with inflammatory etiologies (Supplementary Figure 1A and Table 1) (Bootcov et al., 1997; George et al., 2016; Johnen et al., 2007). Several studies have described GDF15 as playing a role in inflammation-driven states in mice (Abulizi et al.,

2017; Verhamme et al., 2017; Wu et al., 2018). Over the past decade, evidence has emerged in genetic knockout systems that GDF15 may be involved in body weight regulation and metabolic health (Macia et al., 2012; Tsai et al., 2015; Tsai et al., 2013; Tsai et al., 2014). These reports have recently been corroborated by identification of GDNF Family Receptor Alpha Like (GFRAL) as the GDF15 receptor and the finding that this receptor is necessary for the appetite suppressing effects of GDF15 (Emmerson et al., 2017; Hsu et al., 2017; Mullican et al., 2017; Yang et al., 2017). Interestingly, to date, GFRAL has only been shown to be expressed in a small population of cells in the area postrema (AP), suggesting that the effects of GDF15 may be mediated through the brain stem (Hsu et al., 2017). These data are supported by evidence that the anorectic effect of GDF15 requires an intact AP and nucleus of the solitary tract (NTS) (Tsai et al., 2014). Additionally, it has been shown that GDF15 may be able to drive some components of the anorexia-associated metabolic program independent of appetite suppression (Hsu et al., 2017). Together, these data motivated our interest in GDF15 as a potential inflammation-induced mediator of tolerance through metabolic reprogramming. Here we report that GDF15 promotes survival in the settings of acute inflammation. This protective effect is dependent, at least in part, on the stimulation of hepatic sympathetic outflow, promoting triglyceride production. This, in turn, supports metabolic demands of the heart and prevents heart damage and cardiac failure.

Results

GDF15 is induced in inflammatory conditions

Using human serum samples, we found that serum GDF15 is highly abundant in patients with sepsis (Figure 1A). We were able to subset sepsis patients based on the type of infection (bacterial, viral, or both) and found that GDF15 levels were elevated in all cases (Figure 1A), suggesting that it was a common feature of infection-induced inflammation (Supplemental Table 2). Consistent with this, we found that GDF15 was also increased in lupus and autoimmune hepatitis patient serum, albeit to a lower level than in sepsis (Supplemental Figure 1B). We then asked if GDF15 could be induced in murine models by stimuli that mimic a variety of biologically relevant environmental challenges (Figure 1B). Consistent with our human studies, we found that injection of mice with either lipopolysaccharide (LPS) or polyinosinic:polycytidylic acid (Poly (I:C)), which mimic bacterially-induced and virally-induced inflammation, respectively, led to robust increases in plasma levels of GDF15 (Figure 1B). Other types of environmental challenges, including xenobiotic (TCDD) and emetic (LiCl) exposure, cold challenge, and fasting, did not induce GDF15 (Figure 1B) (Spencer et al., 2012). Transcriptionally, *Gdf15* was induced in multiple tissues after inflammatory challenge with LPS, with the highest expression observed in liver and kidney (Figure 1C). *Gfral*, encoding the recently elucidated receptor for GDF15, was found to only be significantly expressed in the hindbrain, as previously described (Figure 1D). Importantly, expression was not induced by LPS in any tissue surveyed suggesting that any effect of manipulating the GDF15 pathway is likely mediated through activation of GFRAL-expressing neurons in the area postrema (Figure 1D). Within the liver, LPS induced *Gdf15* transcription in both $CD45^+$ $CD11b^+$ myeloid cells as well as in $CD45^-$ $CD11b^-$ non-hematopoietic cells (Figure 1E). *In vitro*, bone marrow-derived macrophages increased transcription of *Gdf15* in response to LPS, but not treatments mimicking nutrient scarcity

(Figure 1F). Together, these data demonstrate that GDF15 induction is induced subsequent to inflammatory challenges *in vitro* and *in vivo*.

GDF15 is necessary for survival of acute inflammation

To interrogate the importance of GDF15 in the setting of inflammation, we chose to acutely inhibit GDF15 using a GDF15-neutralizing antibody because genetic deletion of GDF15 has been shown to cause developmental differences related to adiposity, energy expenditure, and neuronal maintenance (Strelau et al., 2009; Tsai et al., 2013). Mice were injected with antibody targeting GDF15 or control antibody raised against keyhole limpet hemocyanin (KLH) one day prior to challenge with either LPS or Poly (I:C), which mimic bacterial- and viral-induced sepsis, respectively. In both cases, neutralization of GDF15 led to significantly increased mortality (Figure 2A and 2B). This mortality likely occurred through inhibition of GDF15 action on GFRAL as LPS-induced FOS induction in the area postrema (AP), where GFRAL-expressing neurons reside, was ablated (Figure 2C and 2D). Interestingly, abrogation of GFRAL activation in the AP did not result in reversal of anorexia associated with lethal dose LPS injection (Supplemental Figure 2A) as might be hypothesized based on the role of GDF15 in cancer cachexia (Hsu et al., 2017; Johnen et al., 2007). Given that GFRAL has also been reported to be expressed in the nucleus of the solitary tract (NTS, Mullican et al., 2017), we also assessed FOS staining in the NTS and found that GDF15 blockade did not suppress NTS activity (Supplemental Figure 2B). We did, however, observe that inhibition of GDF15 in the setting of LPS challenge produced global changes in neuronal activity in the brain (Supplemental Video).

Mortality in the LPS and Poly (I:C) models is thought to be an outcome of tissue damage caused by excessive inflammation. As such, the effects of GDF15 blockade must result from either increased inflammation or reduced ability of tissues to tolerate inflammatory damage. To test the first possibility, we measured plasma levels of two inflammatory cytokines, TNF-α and IL-12, over time and found no difference between anti-GDF15 and control treated mice (Figure 2E and 2F). In the Poly (I:C) model, we found that there was no difference in plasma levels of the anti-viral cytokine IFN-α (Figure 2G). These results suggested that the increased mortality observed with GDF15 blockade may be a result of decreased ability of tissues to tolerate inflammatory damage, rather than the consequence of an exaggerated inflammatory response.

GDF15 is dispensable for pathogen control in both bacterial and viral infections

To formally test whether GDF15 was involved in disease tolerance, it was necessary to test whether blockade of GDF15 had a substantive effect on pathogen burden. To do this, we adopted two models: cecal ligation and puncture (CLP) and influenza infection, which are live poly-bacterial and viral infections, respectively. In the CLP model, mice treated with neutralizing antibody against GDF15 prior to CLP displayed increased mortality as compared to mice treated with the control antibody (Figure 3A). Bacterial titers measured from peritoneal lavage fluid were not different between GDF15 blocking antibody treated mice and control antibody treated mice, nor was there any difference in bacterial dissemination into the blood (Figure 3B and 3C). 16S amplification of bacterial ribosomal DNA in various tissues also did not reveal notable differences in bacterial burden

(Supplemental Figure 2C). Similarly, mice treated with GDF15 blocking antibody were more susceptible to influenza infection compared to mice treated with the control antibody (Figure 3D). No differences in viral load between groups were detected in the bronchoalveolar lavage fluid, or in the lung parenchyma (Figure 3E–3G). Collectively, these findings suggest that the protective effect of GDF15 is largely independent of pathogen control, and is likely due to increased tolerance to inflammatory damage.

GDF15 is cardioprotective in both bacterial and viral inflammation

To examine how GDF15 might promote tissue protection from inflammatory damage, we first asked whether any tissues or organs had increased signs of damage or malfunction due to GDF15 blockade in the LPS and Poly (I:C) models. In a previous study, we found that mice treated with glucose after LPS challenge displayed symptoms consistent with tonic-clonic seizure (Wang et al., 2016). However, GDF15 neutralization did not result in this phenotype, suggesting that the brain might not be the limiting organ. Instead, we found that inhibition of GDF15 led to significantly increased levels of a cardiac injury marker, troponin I, 24 hours after LPS and 36 hours after both LPS and Poly (I:C) (Figure 4A). We also found that GDF15 blockade led to significantly increased levels of both creatinine and blood urea nitrogen (BUN), markers of renal injury, but not until 36 hours after LPS and Poly (I:C) (Figure 4B and 4C). In contrast, plasma alanine aminotransferase (ALT) levels were not substantially different between groups (Figure 4D). These data suggest that GDF15 may play an important cardioprotective and renoprotective role. Consistent with the lack of differences in circulating cytokines between control and anti-GDF15 treated animals, we found that there was no difference in expression of inflammatory genes in the heart or in immune cell infiltration into the heart (Figure 4E and Supplemental Figure 3C), indicating that cardiac damage was likely independent of inflammatory magnitude.

Since GDF15 was necessary to survive both bacterial and viral inflammation in every model we tested and produced similar tissue injury patterns, it appeared to be a proximal mediator of inflammatory physiology generally. Thus, we focused in on the LPS model to identify a mechanism by which GDF15 may be affecting tolerance. Because in the LPS model, we observed dramatic elevations in troponin I levels, we hypothesized that the defect in anti-GDF15 antibody treated mice was primarily cardiac. To test cardiac function, we performed transthoracic echocardiograms on mice 24 hours after LPS that had been pre-treated with either GDF15 neutralizing antibody or control antibody. For these studies, given the enhanced susceptibility of anti-GDF15-treated mice to LPS, non-lethal doses of LPS were used to ensure survival through data collection. Consistent with the increase in troponin I levels observed in anti-GDF15 treated mice after LPS, we found that GDF15 blockade significantly decreased left ventricular stroke volume and cardiac output in comparison to control mice (Figure 4F and 4G). To assess dynamic changes in cardiovascular function, we performed continuous invasive hemodynamic monitoring. For these applications, we also used non-lethal doses of LPS given increased susceptibility to LPS associated with surgical implantation of the transducer. Consistent with our static measures using echocardiography and plasma troponinemia, we observed that GDF15 blocking antibody treated mice displayed altered cardiovascular function, including trends towards decreased blood pressure and tachycardia (Supplemental Figure 3A-B). Together, these findings that GDF15 blockade

results in altered cardiovascular physiology and increased injury suggest that GDF15 has a cardioprotective role in inflammatory states.

Finally, in addition to cardiac injury, we also found that mice treated with GDF15 blocking antibody had a significantly depressed body temperature in response to LPS as compared to control antibody treated mice (Figure 4H). In mice and humans, hypothermia is a severe clinical outcome in sepsis and a robust negative prognostic indicator (Drewry et al., 2015; Nemzek et al., 2004; Wiewel et al., 2016).

GDF15 controls hepatic triglyceride metabolism via sympathetic outflow

To investigate the basis for the protective effect of GDF15 against cardiac damage, we assayed multiple metabolic parameters in the setting of LPS challenge with and without GDF15 blockade. We found that blood glucose, plasma non-esterified fatty acids, and plasma beta-hydroxybutyrate levels, which we had previously shown to be important in tolerance of inflammation (Wang et al., 2016), were unaffected by GDF15 blockade (Supplementary Figure 4A-C). We next used an unbiased lipidomics and metabolomics screen, and found that in both LPS and Poly (I:C) models, GDF15 blockade dramatically reduced plasma levels of all identifiable triglyceride species (Figure 5A). We did not note differences in other metabolites (Supplemental Figure 3D).

Decreased triglycerides could be a result of decreased dietary consumption, decreased hepatic production or increased tissue consumption via the actions of lipoprotein lipase (LPL). Since animals treated with LPS are anorectic immediately after LPS regardless of GDF15 status (Supplemental Figure 2A), the only source of circulating triglycerides is from hepatic export. To determine whether the decrease in plasma triglycerides was a consequence of decreased hepatic production, we performed standard lipid tolerance tests using intralipid and hepatic triglyceride secretion assays using the LPL-inhibitor poloxamer (Kotas et al., 2013). We found that anti-GDF15 treated animals had significantly impaired hepatic triglyceride production (Figure 5B) with no effect on peripheral consumption (Figure 5C).

We next considered the mechanistic basis for these observations and hypothesized that in order for *Gfral*-expressing neurons to affect plasma triglyceride levels, they would need to control neurotransmitter output into peripheral tissues involved in triglyceride metabolism. On this basis, we examined levels of norepinephrine, the major post-ganglionic neurotransmitter, from tissues primarily responsible for triglyceride production and consumption (Augustus et al., 2004). We found that GDF15 blockade significantly diminished norepinephrine levels in the liver, with no changes observed in the adipose tissue, heart, or plasma of LPS treated mice, suggesting that GDF15 might control triglyceride availability by increasing hepatic triglyceride secretion via sympathetic outflow (Figure 5D and Supplementary Figure 3E-G).

To directly test if GDF15 could increase hepatic triglyceride production, we injected endotoxemic animals with recombinant GDF15 (rGDF15) and measured plasma triglycerides. rGDF15, when administered 30 minutes prior to poloxamer, was sufficient to increase hepatic triglyceride export (Figure 5E). Based on our observations that GDF15

blockade resulted in reduced hepatic noradrenaline and impaired hepatic triglyceride export, we then tested whether the ability of GDF15 to stimulate hepatic triglyceride secretion depended on adrenergic signaling. Previous work had shown that beta adrenergic receptors were important in hepatic triglyceride metabolism in both homeostatic and inflammatory settings (Bruinstroop et al., 2012; Nonogaki et al., 1995). Thus, we challenged mice lacking beta-adrenergic receptors 1 and 2 (Adrb1/2$^{-/-}$) with LPS and measured hepatic triglyceride production after rGDF15 injection. We observed that rGDF15 effects on hepatic triglyceride secretion required Adrb1 and/or Adrb2 (Figure 5E).

Next, we asked if we could rescue hepatic triglyceride export in anti-GDF15 treated animals with beta-adrenergic agonists. We thus administered isoproterenol, a non-selective beta-adrenergic agonist, to animals in which GDF15 signaling was impaired. Indeed, isoproterenol administration fully rescued hepatic triglyceride export (Figure 5F). Taken together, these data demonstrate that GDF15, which is induced after acute inflammatory insult, drives hepatic triglyceride metabolism by directing sympathetic outflow to the liver.

GDF15-directed triglyceride metabolism maintains cardiac function and survival in endotoxemia

Both the heart and brown adipose tissue in the fasted state depend on lipids as fuel, and animals unable to utilize lipid metabolism are unable to maintain normal fasting adaptation including maintenance of body temperature and cardiac function (Augustus et al., 2006; Goldberg et al., 2012; Putri et al., 2015). Since LPS induces anorexia and an inability to maintain cardiac function (Figure 4F-G) and body temperature (Figure 4H), we next asked if the insufficient triglyceride levels in GDF15-blocked endotoxemic mice was a major driver of mortality.

To test if restoration of plasma triglycerides would be sufficient to rescue GDF15-blocked animals from endotoxemia, we administered triglyceride-rich parenteral supplementation commonly used in intensive care units (Intralipid 20%) to GDF15-blocked mice. We found that intraperitoneal injection of Intralipid twice a day starting two hours after LPS injection reversed the susceptibility to LPS sepsis caused by GDF15 blockade (Figure 6A). Consistent with this finding, we also observed that Intralipid administration was sufficient to correct both cardiac damage and hypothermia (Figure 6B and 6C). To test whether caloric supplementation with other macronutrients would also have a protective effect in GDF15-blocked animals, we administered isocaloric isovolumetric glucose and casein at the same frequency as intralipid after LPS challenge. We found that glucose administration trended towards potentiating mortality while casein had no effect suggesting that the protective effects were not simply due to volume or caloric supplementation (Supplemental Figure S5A). To formally test the effect of volume resuscitation on survival, we supplemented GDF15-blocked and intact animals with intraperitoneal boluses of saline twice daily (Supplemental Figure S5B). While volume resuscitation was sufficient to rescue isotype-treated animals, it trended towards potentiating mortality in anti-GDF15-treated animals, which is consistent with the observed effects of anti-GDF15 on cardiac function (Figure 4).

Interestingly, intralipid administered to isotype-treated animals potentiated mortality, indicating that intralipid did not rescue mice from LPS sepsis generally, but was protective

only in the GDF15-deficient state, when triglyceride levels are reduced (Supplemental Figure S5C). We reasoned that triglyceride levels, as with all critical metabolic substrates, need to be maintained within a homeostatic range, and that, in the absence of a triglyceride export defect, further administration of exogenous triglycerides might cause hypertriglyceridemia-associated toxicity. Since hypertriglyceridemia and the use of intravenous lipids are associated with pancreatitis (Patel et al., 2014; Pedersen et al., 2016), we asked if intralipid administration caused pancreatitis in GDF15-intact mice. Indeed, we found that only GDF15-intact mice had elevated plasma amylase, consistent with pancreatitis (Supplemental Figure S5D), which is likely a reason for the enhanced mortality observed in GDF15-intact mice. Thus, similar to the role of blood glucose in sepsis, where both high levels due to feeding (Wang et al., 2016) and very low levels due to lack of gluconeogenesis (Weis et al., 2017) resulted in mortality, triglyceride levels must be maintained in the right range to have a protective effect.

Finally, since the addition of exogenous catecholamines, and in particular noradrenaline, is the mainstay of the management of septic shock (Avni et al., 2015; Oba and Lone, 2014) and GDF15 appeared to be controlling hepatic noradrenaline outflow, we asked whether injection of GDF15 alone could improve survival outcomes in sepsis models. Indeed, subcutaneous delivery of GDF15 improved outcomes in both sterile and infectious models of sepsis (Figure 6D, 6E and Supplemental Figure 5E), even when administered late in the course of the infectious challenge. To test if the protective effects of rGDF15 depended on adrenergic signaling, we performed rGDF15 rescue experiments in Adrb1/2-deficient animals (Figure 6F). As with hepatic triglyceride export, the protective effects of rGDF15 required intact adrenergic signaling. Collectively, the data presented here suggest that GDF15 is an endocrine hormone that coordinates tolerance to inflammatory damage by maintaining cardiac function and body temperature through regulation of triglyceride metabolism (Figure 7).

Discussion

While disease tolerance as a defense strategy was first described over a century ago, the underlying mechanisms remain poorly understood. In particular, little is known about how tolerance is coordinated on a systemic level. Catecholamines are perhaps the best described example as they act to defend a baseline blood pressure necessary for survival, and therefore promote survival without dramatically altering the immune response. However, sympathetic nervous system activation is a general response to all stresses and it stands to reason that there exist systemic coordinators of tolerance that are specific to particular environmental challenges. Our study demonstrates that GDF15 is a soluble factor that is induced and promotes survival in inflammatory states through central induction of metabolic adaptation. Our report is consistent with several studies that have described GDF15 as playing a cardioprotective role in inflammation-driven states in mice (Abulizi et al., 2017; Kempf et al., 2006; Xu et al., 2006) and seemingly at odds with reports showing that GDF15 is a pathogenic factor (Isa Santos, 2019; Wu et al., 2018). Given the complexity of sepsis physiology and incomplete understanding of the factors which drive mortality, the reasons for these discrepancies are unknown but could reflect developmental differences between constitutive and transient GDF15 deficiency (Strelau et al., 2009; Tsai et al., 2013), or

perhaps reflect different aspects of biology of GDF15. For example, if GDF15 has both cardioprotective role and negatively regulates peritoneal neutrophils recruitment, then the effect of GDF15 on sepsis outcome would depend on which of the two factors (cardioprotection or antimicrobial defense) is limiting.

Induction of GDF15 has been reported in numerous disease states (Figure 1A, Supplemental Figure 1 and Supplementary Table 1). Importantly, the majority of these disease classes, such as cardiovascular diseases, cancers, metabolic disorders, and rheumatic diseases, are associated with inflammation (Bonaterra et al., 2012; Crusz and Balkwill, 2015; Deane and El-Gabalawy, 2014; Hotamisligil, 2006; Ruparelia et al., 2017). We show here that GDF15 is induced in inflammatory states, but not by other tested environmental challenges, including cold and starvation, and that GDF15 can be induced by inflammatory stimuli in both immune cells and parenchymal cells (Figure 1). Very few exceptions exist to this general rule – perhaps the best described of which is the extremely high levels of GDF15 reported in patients with thalassemia, a disease which is not generally associated with elevated inflammatory biomarkers (Tanno et al., 2007). These cases represent excellent opportunities to investigate possible alternative inducers of GDF15 to better understand its biology.

Our study provides further evidence to support the emerging concept that metabolic reprogramming is an essential component of disease tolerance. We did not find a role for GDF15 in affecting the magnitude of the inflammatory response (Figure 2 and 4) or in pathogen control (Figure 3). Indeed, most available evidence, including those presented in this study, suggests that GDF15 is a key component of the stereotypic inflammatory response and plays a role in metabolic adaptation to acute inflammatory stress. The role of inflammation-induced anorexia in disease tolerance has recently been explored in several studies (Rao et al., 2017; Wang et al., 2016; Weis et al., 2017). In response to any environmental challenge, organisms respond both behaviorally (anorexia) and physiologically (fasting metabolism) in a manner consistent with the specific challenge. Thus, it would be predicted that there would be a coordinated physiologic metabolic response accompanying anorexia in response to inflammation. Indeed, we find that GDF15 is involved in coordinating at least one aspect of the physiological response to inflammation through control of triglyceride availability (Figure 5). While it is almost certain that GDF15 is only one of many factors that control inflammation-induced metabolic adaptation, the mechanism by which GDF15 acts exhibits several features that could be common to host defense responses in the face of environmental challenges. The first is the regulation of nutrients that can be delivered in a tissue-specific manner. In order for tissues to use triglycerides circulating within lipoproteins, they must have capillary lumen-facing, glycosylphosphatidylinositol anchored high density lipoprotein binding protein 1-bound LPL (Goulbourne et al., 2014). We show here that GDF15 blockade specifically results in defects in cardiac function and thermogenesis (Figure 4), which are processes driven by the heart and brown adipose tissue, two of the highest LPL expressing tissues (Augustus et al., 2006). Secondly, we find that GDF15 blockade in the setting of LPS-induced sepsis results in suppression of norepinephrine levels in the liver but not the heart, white adipose tissue, or blood. Distribution of sympathetic output is generally thought to be largely an all or nothing response (sympathetic efferents being all activated in any given stressful situations). However, this type of general response would be inconsistent with observations in various

environmental challenges. For example, catecholamines drive both lipolysis and brown adipose tissue thermogenesis, but in the fasted state, only lipolysis is activated while thermogenesis is suppressed (Cahill, 2006; Trayhurn and Jennings, 1988). Indeed, this has been shown to occur through suppression of sympathetic input to the brown adipose tissue mediated by activation of Agouti-Related Peptide (AgRP)-expressing neurons, which classically drive a behavioral response to negative energy balance (Ruan et al., 2014; Steculorum et al., 2016). This example, as well as the findings presented in this study, suggest that the sympathetic response can be regulated in an organ-specific manner with the exception of a fight-or-flight response, which is an extreme version of sympathetic response.

Mortality in sepsis is driven by failure of vital organs. In our previous studies, we observed that interfering with inflammation-induced anorexia in endotoxemia did not lead to enhanced cardiac damage but rather neuronal toxicity and seizure activity through the attenuation of ketogenesis (Wang et al., 2016). We did not observe seizure activity in GDF15-blocked animals, but rather increased cardiac toxicity (Figure 4). GDF15 peaks early during inflammation (Figure 1) as opposed to ketone bodies, which achieve high steady state levels later in the course of inflammation. Indeed, inflammation-induced endocrine factors – including cytokines – peak at different times during the course of inflammation, which suggests non-redundant functions in maintaining organismal adaptation throughout the course of the inflammatory response. Understanding the evolutionary logic and purpose of these endocrine factors, such as GDF15, which appears to be at least important for triglyceride metabolism and thus for the proper functioning of organs highly dependent on lipid fuels, remains an important unresolved problem in inflammatory physiology. From a therapeutic perspective, understanding which endocrine factors primarily support which vital organs during the different phases of the inflammatory response could be an important step in improving sepsis management.

For decades, research aiming to develop therapeutics for acute inflammatory diseases such as sepsis has focused almost entirely on either improving pathogen clearance (increasing resistance) or dampening inflammation (decreasing resistance). Modulation of resistance has many limitations that restrict the strategy’s potential in the setting of acute inflammation. Indeed, countless therapeutic strategies targeting resistance that have been successful in murine models of sepsis have failed to improve, or even exacerbated, mortality in septic patients (Marshall, 2014). In addition to the limitations of targeting resistance, oftentimes the experimental therapy is given as a pre-treatment or in conjunction with the initiation of the preclinical model, which is inconsistent with the clinical timeline of drug delivery in humans. In this study, we demonstrate that exogenous administration of GDF15 well after the initial inflammatory phase of each disease model is sufficient to improve survival rates in both sterile and infectious sepsis models. Further investigation of disease tolerance mechanisms may provide a new class of therapies for acute inflammatory diseases.

Limitations, Caveats and Open Questions

As with most animal studies, these experiments were performed on mice in a single facility and largely on one genetic background (C57BL/6J). The impacts of the microbiota, genetic background, and other facility-specific factors are unknown. Moreover, unnatural settings

such as those in animal facilities may affect the interpretation of studies in organismal physiology such as this one. Given the wide associations of GDF15 with a variety of biological processes, including pregnancy, metabolism and inflammation, it is very likely that GDF15 plays additional roles to those described in our studies. It is also possible that GFRAL may be expressed on other neurons or even other rare cell types outside of the AP and that additional receptors for GDF15 may exist but have not yet been discovered. There are a number of open questions raised by our study. What other effects are induced by GDF15 and how do they affect the outcomes of acute and chronic inflammation? How does GDF15 signaling in AP result in specific sympathetic output? What are the factors that coordinate allocation of key macronutrients so that organ's metabolic demands are adequately matched with organismal supply? Finally, the therapeutic applicability of this pathway to patients is yet to be determined.

STAR METHODS

Lead Contact and Materials and Availability

Further information and requests for reagents may be directed to, and will be fulfilled by, the lead contact Ruslan Medzhitov (ruslan.medzhitov@yale.edu) or by Andrew Wang (andrew.wang@yale.edu).

Experimental Model and Subject Details

Mice—All animal experiments were performed in accordance with institutional regulations after protocol review and approval by Yale University's Institutional Animal Care and Use Committee. Male C57BL/6J mice (The Jackson Laboratory Stock No. 000664) and Adrb1/2$^{-/-}$ (The Jackson Laboratory Stock No. 003810) animals between 8 and 10 weeks of age were used for all animal experiments in this study.

For LPS endotoxemia, mice were injected intraperitoneally with either lethal or sub-lethal doses of LPS derived from Escherichia coli 055:B5 (Sigma-Aldrich) diluted in PBS. Dosing varies dramatically from lot to lot. New lots are tested for LD50. In these studies, lethal doses are between 7.5 and 12 mg/kg. Sub-lethal doses are between 2.5 and 5 mg/kg. For the Poly(I:C) viral inflammation model, mice were injected retro-orbitally with 30 mg/kg of high molecular weight Poly(I:C) (InvivoGen tlrl-pic-5) diluted in 100 μl of normal saline provided by the manufacturer.

Cecal ligation and puncture was performed similarly to previously described (Toscano et al., 2011). Briefly, mice were anesthetized with a ketamine/xylazine mixture. A 1 to 2 cm midline laparotomy was performed and the cecum was exposed. The cecum was ligated with 4–0 silk suture (Ethicon) 1 cm from the end of the cecum distal to the intestine, and perforated through-and-through with a 20-gauge needle. The cecum was tucked back into the peritoneum and gentle squeezed to extrude a small amount of fecal contents. The peritoneal wall was closed using 4/0 chromic gut (CP Medical). The skin was closed with surgical glue and staples. Mice were temporarily placed on a heating pad to aid in recovery. Sham operated mice underwent the same procedure except the cecum was not tied and no perforation was made.

For flu infections, influenza virus strain A/WSN/33 was originally obtained from the laboratory of Dr. Akiko Iwasaki and was propagated using MDCK cells as described (Okuda et al., 2001). For influenza infection, mice were anesthetized with a ketamine/xylazine mixture and indicated PFU of influenza in 30 μl PBS was administered intranasally in a dropwise manner.

Fasting was performed by placing mice over wire-bottomed cages with food removed from the hopper for the indicated amount of time. Mice were cold challenged at 4 degrees Celsius for the indicated period of time. 2,3,7,8-Tetrachlorodibenzo-p-dioxin (TCDD, Sigma-Aldrich) was injected intraperitoneally at a dose of 30 μg/kg. Lithium chloride (LiCl, Sigma-Aldrich) was injected intraperitoneally at 125 mg/kg.

For supplementation experiments, intralipid 20% (Sigma-Aldrich) was injected intraperitoneally at 8 ml/kg twice per day starting two hours post-LPS injection and twice daily thereafter. Caseine, glucose and PBS were injected intraperitoneally as previously described (Wang et al., 2016). For beta agonism experiments, isoproterenol (Sigma-Aldrich) was dissolved in PBS and injected at 10 mg/kg intraperitoneally. Core body temperature was measured by rectal probe thermometry (Physitemp TH-5 Thermalert).

Method Details

Anti-GDF15 antibody and recombinant GDF15—Control antibody against keyhole limpet hemocyanin and GDF15 blocking antibody (Patent ID: WO2014100689A1, kind gift of Dr. Hui Tian) were given at 10 mg/kg in 100 μl of PBS 16 hours prior to LPS and Poly (I:C) injection, cecal ligation and puncture, or inoculation of influenza. Purified mouse GDF15 were prepared in two ways to independently validate rGDF15 studies. One was generated with methods found in patent ID: WO2012138919A2. The other rGDF15 was produced by the Ring laboratory, which was used to validate key rGDF15 studies where indicated in Figure Legends. Briefly, mature murine GDF15 (amino acids 189–303) was cloned into pD2610-v1 (ATUM Bio) as a C-terminal fusion to the Fc fragment of human IgG1, with an N297A mutation to eliminate all effector functions, and a 3x(GGGGS) linker sequence. Expi293 cells (Thermo Fisher) were transfected with the Fc-GDF15 construct according to the manufacturer's instructions. Protein was purified from the supernatant 96 hours post-transfection using Protein A sepharose (Gold Biotechnology). The column was washed with sterile PBS and eluted using sterile 100 mM glycine pH 3.0. Eluted protein was immediately neutralized with sterile 1 M Tris pH 8.0 and buffer exchanged into sterile PBS using a PD10 column (GE Healthcare). Protein concentration was measured by A280. For survival studies, these proteins were injected subcutaneously into mice at 1 mg/kg starting 6 hours after either LPS injection of CLP and continued daily until completion of the study. For hepatic triglyceride export studies, rGDF15 (1 mg/kg subcutaneous) was injected 30 minutes before poloxamer at 24 hours after LPS challenge.

RNA extraction and quantification—For tissue RNA extraction, tissues were harvested into RNA Bee RNA isolation reagent (Tel-Test, Inc.) and disrupted by bead homogenization (Omni, Inc.). RNA was extracted using the RNeasy Kit according to manufacturer's protocol (Qiagen). cDNA synthesis was performed using MMLV reverse transcriptase (Clontech)

with oligo(dT) primers. qRT-PCR reactions were performed on either a CFX96 Real-Time System or CFX384 Real-Time System (Bio-Rad) using PerfeCTa SYBR Green SuperMix (Quanta Biosciences) and transcript levels were normalized to *Rpl13a*. For measuring *Gfral* expression, Taqman probes were used. Sequence and probe information can be found in Supplemental Table S3.

Cell sorting—For sorting of CD11b+CD45+ and CD11b-CD45- cells from the liver, mice were either treated with a lethal of LPS or vehicle control and sacrificed four hours later. Livers were harvested, finely diced using a razor blade, and incubated in 2 mg/ml Collagenase IV (Worthington Biochemical Corporation) at 37°C under constant agitation for 30 minutes. The resultant suspension was then mechanically forced through a 70-micron cell strainer to generate a single cell suspension and washed prior to staining. Antibodies used for staining are in the key resources table. Cells were sorted on a FACS-Aria (BD) directly into RNA Bee (Tel-Test, Inc.) on a BD FACS Aria.

Flow Cytometry—Single cell suspensions were prepared from the heart exactly as previously described (Pinto et al., 2013). Briefly, animals were euthaized by CO2 and perfused with ice cold HBSS. The heart was excised, minced finely, and placed into freshly prepared Collagenase II (Worthington) and then further digested with Collagenase/Dispase Solution (Roche) and single cells procured and processed for flow cytometry. Antibodies used for flow cytometry are cataloged in the antibodies section of the key resources table. Functional grade mouse anti-CD16/32 (93) antibody was used for Fc-block. At least 1×10^5 cells were acquired on $CD45^+$ cells within the singlet live gate, as defined by size, granularity and pulse-width. Samples were acquired on an LSRII flow cytometer (BD). Fcs files were analyzed using FlowJo (Tree Star Technologies).

Cell culture—Bone marrow derived macrophages (BMDMs) were prepared as previously described (Colegio et al., 2014). For assaying the effect of various stimuli on *Gdf15* expression, BMDMs were plated at a density of 5×10^5 per well in 24-well tissue culture plates. BMDMs either serum starved, treated with 15 mM 2DG (Sigma-Aldrich) treated with 500 μM AICAR (Tocris), treated with 10 ng/ml LPS (Sigma-Aldrich), treated with 10μg/mL R837 (Invivogen) or or Poly (I:C) (InvivoGen).

Immunolabeling-enabled three-dimensional imaging of solvent-cleared organs (iDISCO)—Mice treated with either isotype or GDF15 blocking antibody 16 hours prior to LPS treatment. Four hours after injection with a lethal dose of LPS, mice were fixed by intracardial perfusion of PBS 1X and PFA 4% (Electron Microscopy Sciences). Brains were kept in PFA 4% overnight at 4°C, dissected and cut in the midline. Brains were dehydrated with gradual addition of methanol in water (20%, 40%, 60%, 80%, and 100%, each for 1 hour). Brains were bleached overnight in hydrogen peroxide:methanol in a 1:5 ratio, at 4°C. Brains were gradually rehydrated in water, by removing methanol (80% methanol, 60%, 40%, 20%, and water, each for 1 hour). Brains were then washed in PBS and PBS with 0.2% Triton X-100 (two washes of 1 hour each). Aldehyde groups were blocked by PBS with 0.2% Triton X-100 / 0.3 M glycine (1 day incubation, at 37°C), followed by antigen blocking PBS with 0.2% Triton X-100/6% donkey serum (Jackson Immunoresearch) / 10%

dimethyl sulfoxide (2 days incubation, at 37°C). Brains were then incubated with anti-cFos (Synaptic Systems, 1:200 dilution) for 7 days at 37°C in PBS with 0.2% Tween-20 / 10 μg/mL of heparin / 10% dimethyl sulfoxide and 3% donkey serum. Brains were then thoroughly washed for 1 day in PBS with 0.2% Tween-20 / 10 μg/mL of heparin (5 washes in total). Tissues were then incubated in secondary antibody (Donkey anti-Rabbit IgG (H+L) Highly Cross-Adsorbed Secondary Antibody, Alexa Fluor 647, Thermo Fisher Scientific, 1:1000 dilution) for 7 days at 37°C in PBS with 0.2% Tween-20 / 10 μg/mL of heparin and 3% donkey serum. Brains were then thoroughly washed for 1 day in PBS with 0.2% Tween-20 / 10 μg/mL of heparin (5 washes in total).

Tissue clearing - samples were gradually dehydrated as described previously. The samples were then delipidated with dichloromethane (Millipore-Sigma) and optically cleared in dibenzyl ether (Millipore-Sigma). Samples were stored in dibenzyl ether.

Microscopy and image processing - images of the brain hemisphere was acquired on a light-sheet ultramiscroscope (Ultramicroscope II, LaVision Biotec), provided by the Cellular Neuroscience, Degeneration and Repair Core Facility at Yale School of Medicine. The ultramicroscope was used with a fixed 2 x/0.5 N.A. MVPLAPO objective, and the tissues were submerged in dibenzyl ether during acquisition. Exposure time was 200 ms for each frame, spaced axially with a 3 μm interval, 16-bit depth. Laser excitation of 640 nm was set at 100% for comparison between groups. Volume visualization was performed using Imaris software (Bitplane), in the In Vivo Imaging Facility at Yale School of Medicine. Using Imaris “spot” tool, single activated $cFos^+$ neurons were manually quantified. Regions of the brain were delineated with Imaris “surface” tool, comparing with “The Mouse Brain in Stereotaxic Coordinates” (Paxinos and Franklin, 4th edition).

Cytokine, metabolite, and tissue injury marker analysis—Whole blood was harvested from mice by retro-orbital bleeding and plasma was isolated using lithium heparin coated plasma separator tubes (BD 365985). Plasma TNFα and IL-12 p40/p70 concentration were assayed by sandwich ELISA using capture antibodies (eBioscience and BD, respectively), biotin-conjugated detection antibodies (eBioscience and BD, respectively), HRP-conjugated streptavidin (BD), and TMB substrate reagent (BD). Plasma IFNα concentrations were assayed using kits according to the manufacturer’s protocols (ThermoFisher Scientific). Plasma Tropinin-I concentration and Alanine Aminotransferase (ALT) activity were assayed using kits according to manufacturers’ protocols (Life Diagnostics and Cayman Chemical, respectively). Plasma creatinine and BUN were assayed using HPLC by The George M. O’Brien Kidney Center at Yale. Tissue and plasma norepinephrine levels were assayed according to manufacturer’s protocols (Eagle Biosciences). Plasma non-esterified fatty acid concentration was measured using a kit according the manufacturer’s protocols (Wako Diagnostics 999–34691, 995–34791, 991–34891, and 993–35191). Plasma β-hydroxybutyrate concentrations were measured using a kit according the manufacturer’s protocols (Cayman Chemical). Amylase was measured using an ELISA kit according to the manufacturer’s protocol (Abcam). Capillary blood glucose was measured according to manufacturer instruction using a blood glucose monitor (BD OneTouch Ultra 2).

Quantification of bacterial and viral loads—Bacterial titers of peritoneal lavage fluid and blood from CLP-treated mice were serially diluted, plated on agar plates, and incubated at 37°C overnight. Influenza titers in the lung and bronchoalveolar lavage fluid were determined as previously described (Okuda et al., 2001).

Bacterial load in tissues of interest was examined using an absolute quantification qPCR assay, amplifying the V4 region of the 16S rRNA gene (primer sequences in Supplemental Table S3 (Kozich et al., 2013)). The standard curve for this assay was prepared as follows: an overnight E. coli culture (strain B23113 from NRRL-USDA) was enumerated by correlating OD600 values with traditional spread plating CFU counts on LB agar. This correlation curve was utilized to take a subsequent fresh E. coli culture and dilute it to known concentrations (10^9 – 10^2 CFU/mL), then extracting gDNA from 1mL of each dilution using Qiagen's DNeasy UltraClean Microbial Kit. This same kit was used to extract bacterial gDNA from animal tissues according to the manufacturer's protocol, which were then run by qPCR and interpolated to the CFU/mL standard curve.

Hepatic Triglyceride Secretion and Lipid Tolerance Test—Intravenous fat tolerance tests were performed by injecting mice with 100 μL of Intralipid 20% and then measuring triglycerides at the indicated time points. To measure hepatic lipid export, mice were injected with 1 g/kg poloxamer 407 (Pluronic F-127, Sigma), and plasma was collected at the indicated time points for analysis.

Transthoracic echocardiogram (TTE)—Animals were anesthetized with inhaled 2% isoflurane/ O2 (v/v) in a chamber. During imaging recording, 1–1.5% isoflurane/O2 (v/v) was provided. Animals were kept in supine position on 37ºC heating platforms. Images were recorded along the parasternal long axis and short axis in the middle part of the left ventricle. Images were analyzed with Visual Sonics Vevo 2100 high-resolution ultrasound imaging system. Ejection fraction, end diastolic volume, stroke volume and cardiac output were obtained from M-Mode and AM-Mode parasternal long axis and short axis measurements. Ultrasound images were recorded and analyzed by an experienced technologist with expertise in human and mouse ultrasound imaging. The technologist was completely blind to the treatments administered in this study.

Ambulatory blood pressure transducer implantation—A blood pressure transducer (TA11-PA-C10, commercially available through Data Sciences International) was surgically implanted under isoflurane anesthesia (1–3% in oxygen) into the carotid artery of mice using sterile surgical technique. Post-operative analgesics (Meloxicam) were provided for 48 hours. The skin was closed with surgical staples and the mouse allowed to recover for approximately 7 days. Afterwards, surgical staples were removed, the mice were transferred to a fresh cage (singly housed for data collection), and allowed to acclimate for several days prior to initiation of study. Any test substances were administered under brief isoflurane anesthesia. A 10 second segment was collected every minute for the duration of the experiment.

Lipidomics—Lipidomics was performed by the West Coast Metabolomics Center at UC Davis. Briefly, the lipidomics workflow involves sample extraction in MTBE with addition

of internal standards, followed by ultra high pressure liquid chromatography (UHPLC) on a Waters CSH column, interfaced to a QTOF mass spectrometer (high resolution, accurate mass), with a 15 minute total run time. Data are collected in both positive and negative ion mode, and analyzed using MassHunter (Agilent). Approximately 400 lipids can be identified from plasma, with additional unknowns. The method is highly stable and has been validated on large datasets (>8,000 samples) collected over long time periods (> 1 year). Counts of each lipid species for each sample from GDF15 blocking antibody-treated mice was normalized to the average of counts for the corresponding lipid species in isotype-treated mice and $\log_2$ fold change was determined. Resulting values were clustered using Cluster 3.0 by lipid species. Heatmaps were generated in Java TreeView.

Quantification and Statistical Analysis

Results were statistically analyzed using Student's *t* test or an analysis of variance (ANOVA) test with multiple comparisons where appropriate using Prism 6.0 (GraphPad Software, Inc). Kaplan Meier survival curves were compared using log-rank Mantel-Cox test. A p value of < 0.05 was considered to be statistically significant.

Supplementary Material

Refer to Web version on PubMed Central for supplementary material.

ACKNOWLEDGMENTS

We thank members of the Medzhitov and Wang labs for helpful discussions. GDF15 blocking antibody was a kind gift of Dr. Hui Tian of NGM Biopharmaceuticals. We thank Dr. Sarah Huen of UT Southwestern for her constructive feedback of the manuscript. We thank Dr. Noah Palm and Tyler Rice for assistance with 16S quantification. Autoimmune hepatitis samples were procured from the Yale University Liver Center which is supported by the National Institute of Diabetes and Digestive and Kidney Diseases of the National Institutes of Health under Award Number P30KD034989. Plasma samples were procured by the Yale MICU repository. Processing support and long term sample storage and maintenance was provided by The Yale Lung Repository funded in part by HL 109233 and HL 125850. All samples were obtained after informed consent in protocols approved by the Yale Institutional Review Board. Plasma creatinine and BUN samples as well as invasive hemodynamic telemetric monitoring were performed through the George M. O'Brien Kidney Center at Yale (NIH Grant P30-DK079310). Support was provided by the HHMI, Else Kröner Fresenius Foundation, and The Blavatnik Family Foundation (R.M.), the NIH Grant 1R01AI144152–01 (R.M. and A.W.), and the NIH Clinical Investigator Award K08AI128745 (A.W.).

REFERENCES

Abulizi P, Loganathan N, Zhao D, Mele T, Zhang Y, Zwiep T, Liu K, and Zheng X. (2017). Growth Differentiation Factor-15 Deficiency Augments Inflammatory Response and Exacerbates Septic Heart and Renal Injury Induced by Lipopolysaccharide. Sci Rep 7, 1037. [PubMed: 28432312]

Angus DC, and van der Poll T. (2013). Severe sepsis and septic shock. The New England journal of medicine 369, 840–851. [PubMed: 23984731]

Anrather J, and Iadecola C. (2016). Inflammation and Stroke: An Overview. Neurotherapeutics 13, 661–670. [PubMed: 27730544]

Augustus A, Yagyu H, Haemmerle G, Bensadoun A, Vikramadithyan RK, Park SY, Kim JK, Zechner R, and Goldberg IJ (2004). Cardiac-specific knock-out of lipoprotein lipase alters plasma lipoprotein triglyceride metabolism and cardiac gene expression. The Journal of biological chemistry 279, 25050–25057. [PubMed: 15028738]

Augustus AS, Buchanan J, Park TS, Hirata K, Noh HL, Sun J, Homma S, D'Armiento J, Abel ED, and Goldberg IJ (2006). Loss of lipoprotein lipase-derived fatty acids leads to increased cardiac glucose

metabolism and heart dysfunction. The Journal of biological chemistry 281, 8716–8723. [PubMed: 16410253]

Avni T, Lador A, Lev S, Leibovici L, Paul M, and Grossman A. (2015). Vasopressors for the Treatment of Septic Shock: Systematic Review and Meta-Analysis. PLoS One 10, e0129305. [PubMed: 26237037]

Ayres JS, Freitag N, and Schneider DS (2008). Identification of Drosophila mutants altering defense of and endurance to Listeria monocytogenes infection. Genetics 178, 1807–1815. [PubMed: 18245331]

Ayres JS, and Schneider DS (2012). Tolerance of infections. Annual review of immunology 30, 271–294.

Bonaterra GA, Zugel S, Thogersen J, Walter SA, Haberkorn U, Strelau J, and Kinscherf R. (2012). Growth differentiation factor-15 deficiency inhibits atherosclerosis progression by regulating interleukin-6-dependent inflammatory response to vascular injury. J Am Heart Assoc 1, e002550. [PubMed: 23316317]

Bootcov MR, Bauskin AR, Valenzuela SM, Moore AG, Bansal M, He XY, Zhang HP, Donnellan M, Mahler S, Pryor K, et al. (1997). MIC-1, a novel macrophage inhibitory cytokine, is a divergent member of the TGF-beta superfamily. Proceedings of the National Academy of Sciences of the United States of America 94, 11514–11519.

Bruinstroop E, Pei L, Ackermans MT, Foppen E, Borgers AJ, Kwakkel J, Alkemade A, Fliers E, and Kalsbeek A. (2012). Hypothalamic neuropeptide Y (NPY) controls hepatic VLDL-triglyceride secretion in rats via the sympathetic nervous system. Diabetes 61, 1043–1050. [PubMed: 22461566]

Cahill GF Jr. (2006). Fuel metabolism in starvation. Annu Rev Nutr 26, 1–22. [PubMed: 16848698]

Colegio OR, Chu N-Q, Szabo AL, Chu T, Rhebergen AM, Jairam V, Cyrus N, Brokowski CE, Eisenbarth SC, Phillips GM, et al. (2014). Functional polarization of tumour-associated macrophages by tumour-derived lactic acid. Nature 513, 559–563. [PubMed: 25043024]

Crusz SM, and Balkwill FR (2015). Inflammation and cancer: advances and new agents. Nat Rev Clin Oncol 12, 584–596. [PubMed: 26122183]

de Groot H, and Rauen U. (2007). Ischemia-reperfusion injury: processes in pathogenetic networks: a review. Transplant Proc 39, 481–484. [PubMed: 17362763]

Deane KD, and El-Gabalawy H. (2014). Pathogenesis and prevention of rheumatic disease: focus on preclinical RA and SLE. Nat Rev Rheumatol 10, 212–228. [PubMed: 24514912]

Drewry AM, Fuller BM, Skrupky LP, and Hotchkiss RS (2015). The presence of hypothermia within 24 hours of sepsis diagnosis predicts persistent lymphopenia. Crit Care Med 43, 1165–1169. [PubMed: 25793436]

Emmerson PJ, Wang F, Du Y, Liu Q, Pickard RT, Gonciarz MD, Coskun T, Hamang MJ, Sindelar DK, Ballman KK, et al. (2017). The metabolic effects of GDF15 are mediated by the orphan receptor GFRAL. Nat Med 23, 1215–1219. [PubMed: 28846098]

Frangogiannis NG (2014). The inflammatory response in myocardial injury, repair, and remodelling. Nat Rev Cardiol 11, 255–265. [PubMed: 24663091]

George M, Jena A, Srivatsan V, Muthukumar R, and Dhandapani VE (2016). GDF 15--A Novel Biomarker in the Offing for Heart Failure. Curr Cardiol Rev 12, 37–46. [PubMed: 26750722]

Goldberg IJ, Trent CM, and Schulze PC (2012). Lipid metabolism and toxicity in the heart. Cell Metab 15, 805–812. [PubMed: 22682221]

Goulbourne CN, Gin P, Tatar A, Nobumori C, Hoenger A, Jiang H, Grovenor CR, Adeyo O, Esko JD, Goldberg IJ, et al. (2014). The GPIHBP1-LPL complex is responsible for the margination of triglyceride-rich lipoproteins in capillaries. Cell Metab 19, 849–860. [PubMed: 24726386]

Hotamisligil GS (2006). Inflammation and metabolic disorders. Nature 444, 860–867. [PubMed: 17167474]

Hsu JY, Crawley S, Chen M, Ayupova DA, Lindhout DA, Higbee J, Kutach A, Joo W, Gao Z, Fu D, et al. (2017). Non-homeostatic body weight regulation through a brainstem-restricted receptor for GDF15. Nature 550, 255–259. [PubMed: 28953886]

Isa Santos HGC, Ana Neves-Costa, Elsa Seixas, Tiago R. Velho, Dora Pedroso, André Barros, Rui Martins, Nuno Carvalho, Didier Payen, Sebastian Weis, Hyon-Seung Yi, Minho Shong, View

ORCID ProfileLuís Ferreira Moita (2019). CXCL5-mediated recruitment of neutrophils into the peritoneal cavity of Gdf15-deficient mice protects against abdominal sepsis. bioRxiv.

Johnen H, Lin S, Kuffner T, Brown DA, Tsai VW, Bauskin AR, Wu L, Pankhurst G, Jiang L, Junankar S, et al. (2007). Tumor-induced anorexia and weight loss are mediated by the TGF-beta superfamily cytokine MIC-1. Nat Med 13, 1333–1340. [PubMed: 17982462]

Kempf T, Eden M, Strelau J, Naguib M, Willenbockel C, Tongers J, Heineke J, Kotlarz D, Xu J, Molkentin JD, et al. (2006). The transforming growth factor-beta superfamily member growth-differentiation factor-15 protects the heart from ischemia/reperfusion injury. Circ Res 98, 351–360. [PubMed: 16397141]

Kotas ME, Jurczak MJ, Annicelli C, Gillum MP, Cline GW, Shulman GI, and Medzhitov R. (2013). Role of caspase-1 in regulation of triglyceride metabolism. Proceedings of the National Academy of Sciences of the United States of America 110, 4810–4815.

Kozich JJ, Westcott SL, Baxter NT, Highlander SK, and Schloss PD (2013). Development of a dual-index sequencing strategy and curation pipeline for analyzing amplicon sequence data on the MiSeq Illumina sequencing platform. Appl Environ Microbiol 79, 5112–5120. [PubMed: 23793624]

Macia L, Tsai VW, Nguyen AD, Johnen H, Kuffner T, Shi YC, Lin S, Herzog H, Brown DA, Breit SN, et al. (2012). Macrophage inhibitory cytokine 1 (MIC-1/GDF15) decreases food intake, body weight and improves glucose tolerance in mice on normal & obesogenic diets. PLoS One 7, e34868. [PubMed: 22514681]

Marshall JC (2014). Why have clinical trials in sepsis failed? Trends Mol Med 20, 195–203. [PubMed: 24581450]

Medzhitov R, Schneider DS, and Soares MP (2012). Disease Tolerance as a Defense Strategy. Science (New York, NY) 335, 936–941.

Mullican SE, Lin-Schmidt X, Chin CN, Chavez JA, Furman JL, Armstrong AA, Beck SC, South VJ, Dinh TQ, Cash-Mason TD, et al. (2017). GFRAL is the receptor for GDF15 and the ligand promotes weight loss in mice and nonhuman primates. Nat Med 23, 1150–1157. [PubMed: 28846097]

Nemzek JA, Xiao HY, Minard AE, Bolgos GL, and Remick DG (2004). Humane endpoints in shock research. Shock 21, 17–25. [PubMed: 14676679]

Nonogaki K, Moser AH, Pan XM, Staprans I, Grunfeld C, and Feingold KR (1995). Lipoteichoic acid stimulates lipolysis and hepatic triglyceride secretion in rats in vivo. Journal of lipid research 36, 1987–1995. [PubMed: 8558086]

Oba Y, and Lone NA (2014). Mortality benefit of vasopressor and inotropic agents in septic shock: a Bayesian network meta-analysis of randomized controlled trials. J Crit Care 29, 706–710. [PubMed: 24857641]

Okuda K, Ihata A, Watabe S, Okada E, Yamakawa T, Hamajima K, Yang J, Ishii N, Nakazawa M, Okuda K, et al. (2001). Protective immunity against influenza A virus induced by immunization with DNA plasmid containing influenza M gene. Vaccine 19, 3681–3691. [PubMed: 11395202]

Patel KS, Noel P, and Singh VP (2014). Potential influence of intravenous lipids on the outcomes of acute pancreatitis. Nutr Clin Pract 29, 291–294. [PubMed: 24687866]

Pedersen SB, Langsted A, and Nordestgaard BG (2016). Nonfasting Mild-to-Moderate Hypertriglyceridemia and Risk of Acute Pancreatitis. JAMA Intern Med 176, 1834–1842. [PubMed: 27820614]

Pinto AR, Chandran A, Rosenthal NA, and Godwin JW (2013). Isolation and analysis of single cells from the mouse heart. J Immunol Methods 393, 74–80. [PubMed: 23578979]

Putri M, Syamsunarno MR, Iso T, Yamaguchi A, Hanaoka H, Sunaga H, Koitabashi N, Matsui H, Yamazaki C, Kameo S, et al. (2015). CD36 is indispensable for thermogenesis under conditions of fasting and cold stress. Biochemical and biophysical research communications 457, 520–525. [PubMed: 25596128]

Raberg L, Sim D, and Read AF (2007). Disentangling genetic variation for resistance and tolerance to infectious diseases in animals. Science 318, 812–814. [PubMed: 17975068]

Rao S, Schieber AMP, O'Connor CP, Leblanc M, Michel D, and Ayres JS (2017). Pathogen-Mediated Inhibition of Anorexia Promotes Host Survival and Transmission. Cell 168, 503–516e512. [PubMed: 28129542]

Ruan HB, Dietrich MO, Liu ZW, Zimmer MR, Li MD, Singh JP, Zhang K, Yin R, Wu J, Horvath TL, et al. (2014). O-GlcNAc transferase enables AgRP neurons to suppress browning of white fat. Cell 159, 306–317. [PubMed: 25303527]

Ruparelia N, Chai JT, Fisher EA, and Choudhury RP (2017). Inflammatory processes in cardiovascular disease: a route to targeted therapies. Nat Rev Cardiol 14, 314. [PubMed: 28300082]

Salmon SC, and Laude HH (1932). Twenty years of testing varieties and strains of winter wheat at the Kansas Agricultural Experiment Station. Kansas Agricultural Experimental Station Bulletin.

Sanchez KK, Chen GY, Schieber AMP, Redford SE, Shokhirev MN, Leblanc M, Lee YM, and Ayres JS (2018). Cooperative Metabolic Adaptations in the Host Can Favor Asymptomatic Infection and Select for Attenuated Virulence in an Enteric Pathogen. Cell 175, 146–158e115. [PubMed: 30100182]

Schafer JF (1971). Tolerance to plant disease. Annual Reviews Phytopathology 9, 235–252.

Soares MP, Teixeira L, and Moita LF (2017). Disease tolerance and immunity in host protection against infection. Nat Rev Immunol 17, 83–96. [PubMed: 28044057]

Spencer CM, Eckel LA, Nardos R, and Houpt TA (2012). Area postrema lesions attenuate LiCl-induced c-Fos expression correlated with conditioned taste aversion learning. Physiol Behav 105, 151–160. [PubMed: 21889521]

Steculorum SM, Ruud J, Karakasilioti I, Backes H, Engstrom Ruud L, Timper K, Hess ME, Tsaousidou E, Mauer J, Vogt MC, et al. (2016). AgRP Neurons Control Systemic Insulin Sensitivity via Myostatin Expression in Brown Adipose Tissue. Cell 165, 125–138. [PubMed: 27015310]

Strelau J, Strzelczyk A, Rusu P, Bendner G, Wiese S, Diella F, Altick AL, von Bartheld CS, Klein R, Sendtner M, et al. (2009). Progressive postnatal motoneuron loss in mice lacking GDF-15. The Journal of neuroscience : the official journal of the Society for Neuroscience 29, 13640–13648. [PubMed: 19864576]

Tanno T, Bhanu NV, Oneal PA, Goh SH, Staker P, Lee YT, Moroney JW, Reed CH, Luban NL, Wang RH, et al. (2007). High levels of GDF15 in thalassemia suppress expression of the iron regulatory protein hepcidin. Nat Med 13, 1096–1101. [PubMed: 17721544]

Toscano MG, Ganea D, and Gamero AM (2011). Cecal ligation puncture procedure. J Vis Exp.

Trayhurn P, and Jennings G. (1988). Nonshivering thermogenesis and the thermogenic capacity of brown fat in fasted and/or refed mice. The American journal of physiology 254, R11–16. [PubMed: 2827526]

Tsai VW, Macia L, Feinle-Bisset C, Manandhar R, Astrup A, Raben A, Lorenzen JK, Schmidt PT, Wiklund F, Pedersen NL, et al. (2015). Serum Levels of Human MIC-1/GDF15 Vary in a Diurnal Pattern, Do Not Display a Profile Suggestive of a Satiety Factor and Are Related to BMI. PLoS One 10, e0133362. [PubMed: 26207898]

Tsai VW, Macia L, Johnen H, Kuffner T, Manadhar R, Jorgensen SB, Lee-Ng KK, Zhang HP, Wu L, Marquis CP, et al. (2013). TGF-b superfamily cytokine MIC-1/GDF15 is a physiological appetite and body weight regulator. PLoS One 8, e55174. [PubMed: 23468844]

Tsai VW, Manandhar R, Jorgensen SB, Lee-Ng KK, Zhang HP, Marquis CP, Jiang L, Husaini Y, Lin S, Sainsbury A, et al. (2014). The anorectic actions of the TGFbeta cytokine MIC-1/GDF15 require an intact brainstem area postrema and nucleus of the solitary tract. PLoS One 9, e100370. [PubMed: 24971956]

van der Poll T, van de Veerdonk FL, Scicluna BP, and Netea MG (2017). The immunopathology of sepsis and potential therapeutic targets. Nat Rev Immunol 17, 407–420. [PubMed: 28436424]

Verhamme FM, Seys LJM, De Smet EG, Provoost S, Janssens W, Elewaut D, Joos GF, Brusselle GG, and Bracke KR (2017). Elevated GDF-15 contributes to pulmonary inflammation upon cigarette smoke exposure. Mucosal Immunol 10, 1400–1411. [PubMed: 28145442]

Wang A, Huen SC, Luan HH, Yu S, Zhang C, Gallezot JD, Booth CJ, and Medzhitov R. (2016). Opposing Effects of Fasting Metabolism on Tissue Tolerance in Bacterial and Viral Inflammation. Cell 166, 1512–1525e1512. [PubMed: 27610573]

Weis S, Carlos AR, Moita MR, Singh S, Blankenhaus B, Cardoso S, Larsen R, Rebelo S, Schauble S, Del Barrio L, et al. (2017). Metabolic Adaptation Establishes Disease Tolerance to Sepsis. Cell 169, 1263–1275e1214. [PubMed: 28622511]

Wiewel MA, Harmon MB, van Vught LA, Scicluna BP, Hoogendijk AJ, Horn J, Zwinderman AH, Cremer OL, Bonten MJ, Schultz MJ, et al. (2016). Risk factors, host response and outcome of hypothermic sepsis. Crit Care 20, 328. [PubMed: 27737683]

Wu Q, Jiang D, Schaefer NR, Harmacek L, O'Connor BP, Eling TE, Eickelberg O, and Chu HW (2018). Overproduction of growth differentiation factor 15 promotes human rhinovirus infection and virus-induced inflammation in the lung. Am J Physiol Lung Cell Mol Physiol 314, L514–L527. [PubMed: 29192094]

Xu J, Kimball TR, Lorenz JN, Brown DA, Bauskin AR, Klevitsky R, Hewett TE, Breit SN, and Molkentin JD (2006). GDF15/MIC-1 functions as a protective and antihypertrophic factor released from the myocardium in association with SMAD protein activation. Circ Res 98, 342–350. [PubMed: 16397142]

Yang L, Chang CC, Sun Z, Madsen D, Zhu H, Padkjaer SB, Wu X, Huang T, Hultman K, Paulsen SJ, et al. (2017). GFRAL is the receptor for GDF15 and is required for the anti-obesity effects of the ligand. Nat Med 23, 1158–1166. [PubMed: 28846099]

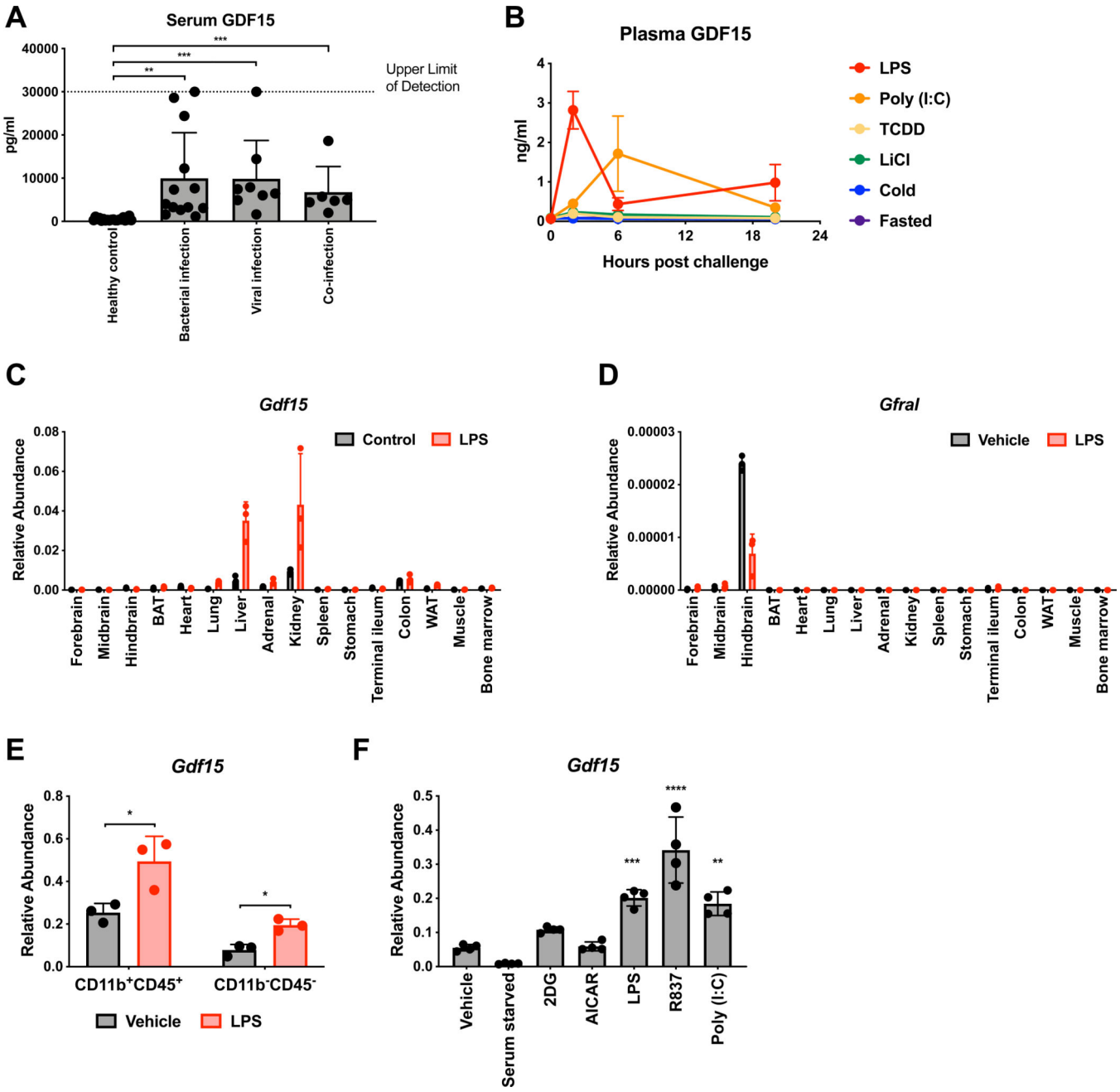

Figure 1. GDF15 is induced in inflammatory states.

(A) Serum GDF15 levels in either healthy humans or humans with culture and/or PCR-proven infections hospitalized in the intensive care unit.

(B) Plasma GDF15 levels in mice 0, 2, 6, and 20 hours after exposure to one of the indicated challenges (n>4 per group per time point, representative of 2 experiments)

(C) *Gdf15* expression levels in the indicated tissues three hours after either vehicle or LPS treatment. Abundance is relative to *Rpl13a* expression. (n=3 per group, representative of 2 experiments)

(D) *Gfral* expression levels in the indicated tissues three hours after either vehicle or LPS treatment. Abundance is relative to *Rpl13a* expression. (n=3 per group, representative of 2 experiments)

(E) *Gdf15* expression levels in either $CD11b^{+}CD45^{+}$ myeloid cells or $C11b^{-}CD45^{-}$ parenchymal cells in the liver three hours after either vehicle or LPS treatment. Abundance is relative to *Rpl13a* expression. (n=3 per group, representative of 2 experiments)

(F) *Gdf15* expression levels in bone marrow-derived macrophages (BMDMs) one hour after exposure to the indicated treatments. Abundance is relative to *Rpl13a* expression. (n=4 per group, representative of 3 experiments)

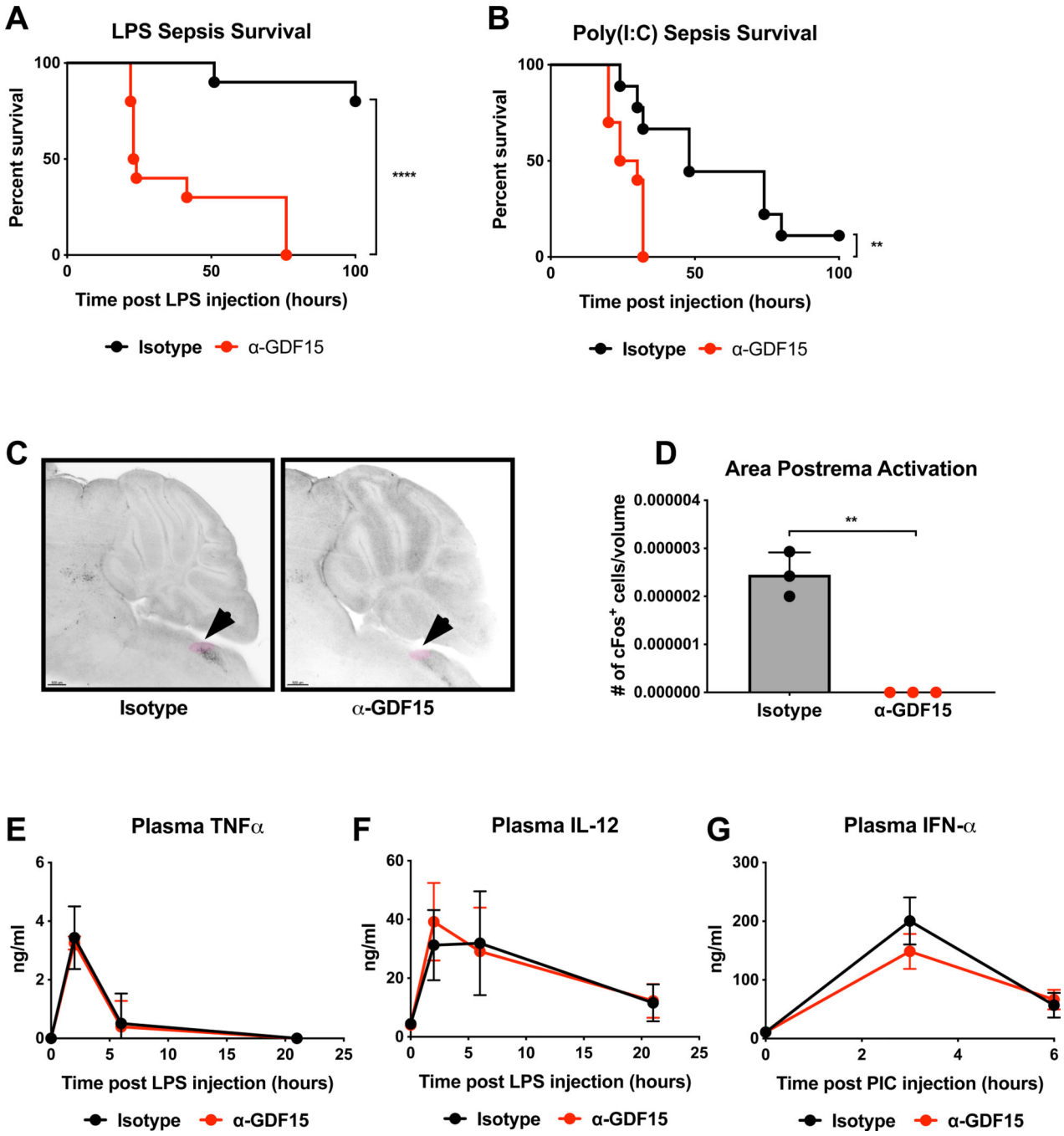

Figure 2. GDF15 is required for survival of acute inflammatory states.

(A) Survival after intraperitoneal injection of LPS following pre-treatment with either isotype or α-GDF15 antibody. (n=10 per group)

(B) Survival after retro-orbital injection of Poly(I:C) following pre-treatment with either isotype or α-GDF15 antibody. (n>9 per group)

(C) Images of cFos staining in the area postrema (AP, highlighted in pink) four hours after intraperitoneal injection of LPS following pre-treatment with either isotype or α-GDF15 antibody.

(D) Quantification of cFos staining in the area postrema four hours after intraperitoneal injection of LPS following pre-treatment with either isotype or α-GDF15 antibody.
(E) Plasma TNFα levels in mice 0, 2, 6, and 21 hours after intraperitoneal injection of LPS following pre-treatment with either isotype or α-GDF15 antibody. (n>4 per group)
(F) Plasma IL-12 levels in mice 0, 2, 6, and 21 hours after intraperitoneal injection of LPS following pre-treatment with either isotype or α-GDF15 antibody. (n>4 per group)
(G) Plasma IFNα levels in mice 0, 3, and 6 hours after retro-orbital injection of Poly(I:C) following pre-treatment with either isotype or α-GDF15 antibody. (n>5 per group)

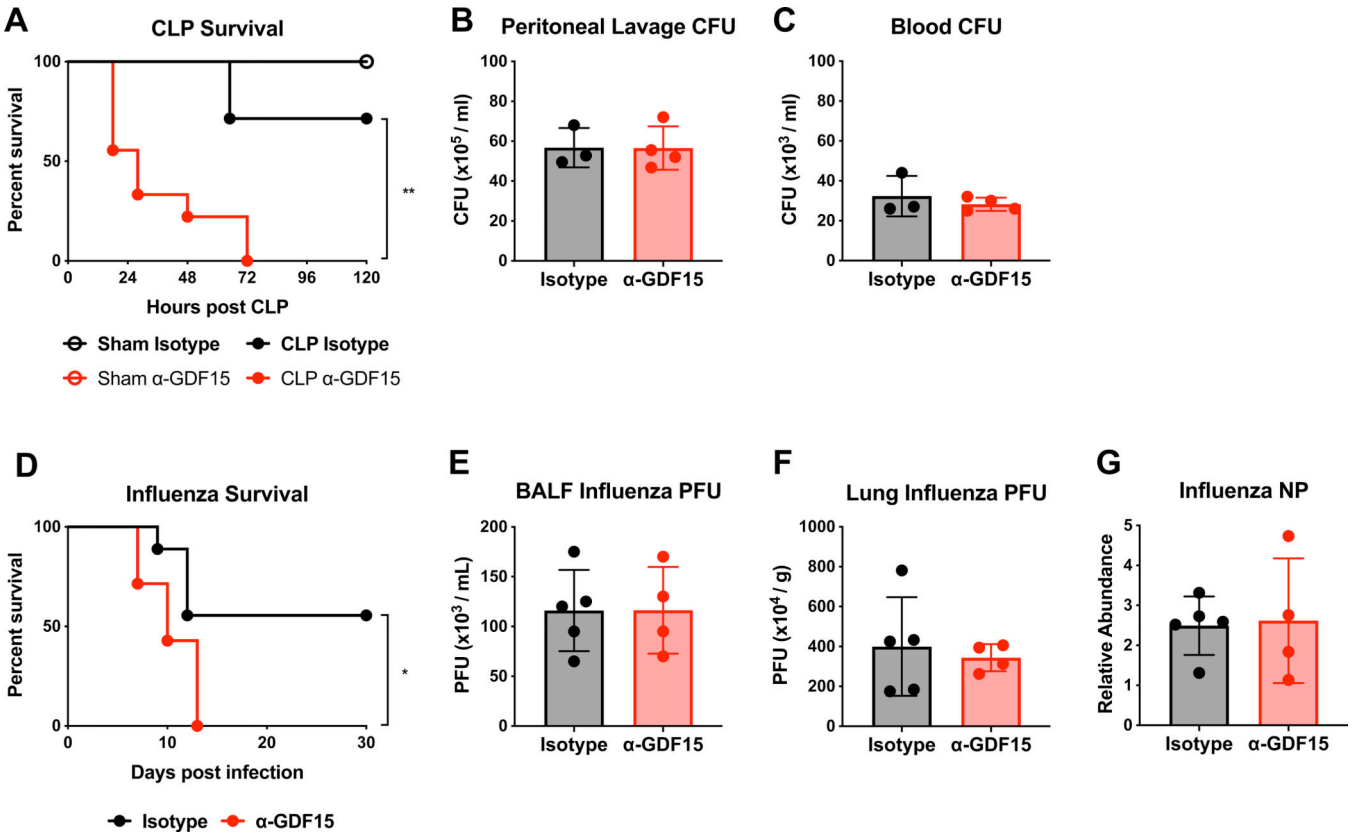

Figure 3. GDF15 promotes survival of acute inflammatory states through disease tolerance.

(A) Survival after either cecal ligation and puncture (CLP) or sham operation following pre-treatment with either isotype or α-GDF15 antibody. (n>5 per group, representative of 2 experiments)

(B) Colony-forming units (CFUs) cultured from mouse peritoneal lavage fluid 24 hours after CLP following pre-treatment with either isotype or α-GDF15 antibody.

(C) CFUs cultured from mouse blood 24 hours after CLP following pre-treatment with either isotype or α-GDF15 antibody.

(D) Survival after infection with influenza strain A/WSN/33 following pre-treatment with either isotype or α-GDF15 antibody and continued bi-weekly antibody treatment. (n>7 per group)

(E) Plaque-forming units (PFUs) isolated from mouse bronchoalveolar lavage fluid (BALF) 6 days after infection with influenza strain A/WSN/33 following pre-treatment with either isotype or α-GDF15 antibody and continued bi-weekly antibody treatment.

(F) Plaque-forming units (PFUs) isolated from lung parenchyma 6 days after infection with influenza strain A/WSN/33 following pre-treatment with either isotype or α-GDF15 antibody and continued bi-weekly antibody treatment.

(G) Influenza NP expression levels in lung parenchyma 6 days after infection with influenza strain A/WSN/33 following pre-treatment with either isotype or α-GDF15 antibody and continued bi-weekly antibody treatment. Abundance is relative to *Rpl13a* expression.

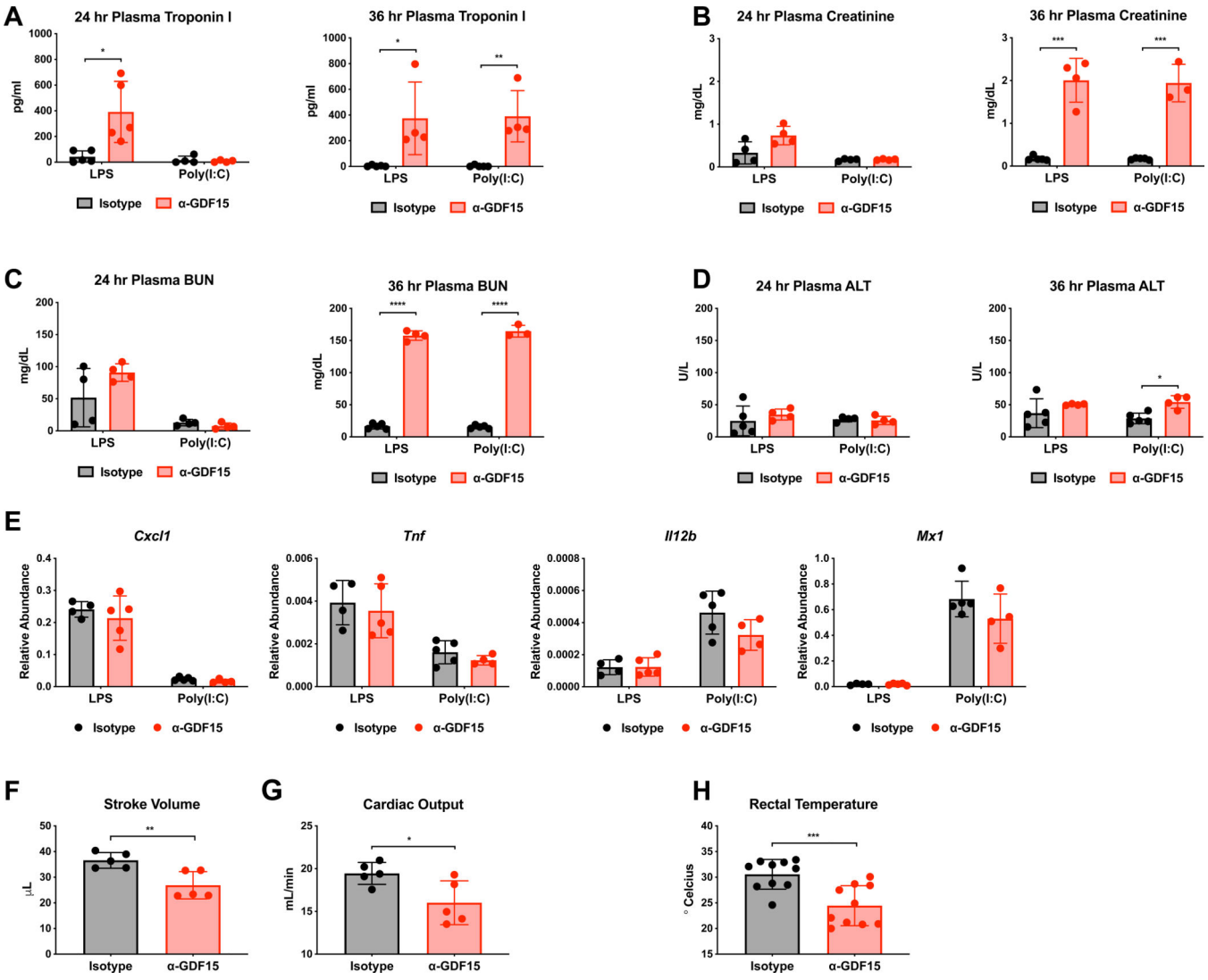

Figure 4. Blockade of GDF15 in acute inflammatory states results in defects cardiac and thermal homeostasis.

(A) Plasma troponin I levels 24 and 36 hours after either LPS or Poly(I:C) injection following pre-treatment with either isotype or α-GDF15 antibody.

(B) Plasma creatinine levels 24 and 36 hours after either LPS or Poly(I:C) injection following pre-treatment with either isotype or α-GDF15 antibody.

(C) Plasma blood urea nitrogen (BUN) levels 24 and 36 hours after either LPS or Poly(I:C) injection following pre-treatment with either isotype or α-GDF15 antibody.

(D) Plasma alanine aminotransferase (ALT) levels 24 and 36 hours after either LPS or Poly(I:C) injection following pre-treatment with either isotype or α-GDF15 antibody.

(E) *Cxcl1*, *Tnf*, *Il12b*, *Mx1* expression levels in heart tissue 8 hours after injection of either LPS or Poly(I:C) following pre-treatment with either isotype or α-GDF15 antibody. Abundance is relative to *Rpl13a* expression.

(F) Stroke volume as measured by trans-thoracic echocardiogram 24 hours after LPS injection following pre-treatment with either isotype or α-GDF15 antibody.

(G) Cardiac output calculated from trans-thoracic echocardiogram measurements 24 hours after LPS injection following pre-treatment with either isotype or α-GDF15 antibody.
(H) Rectal temperature in mice 20 hours after LPS injection following pre-treatment with either isotype or α-GDF15 antibody.

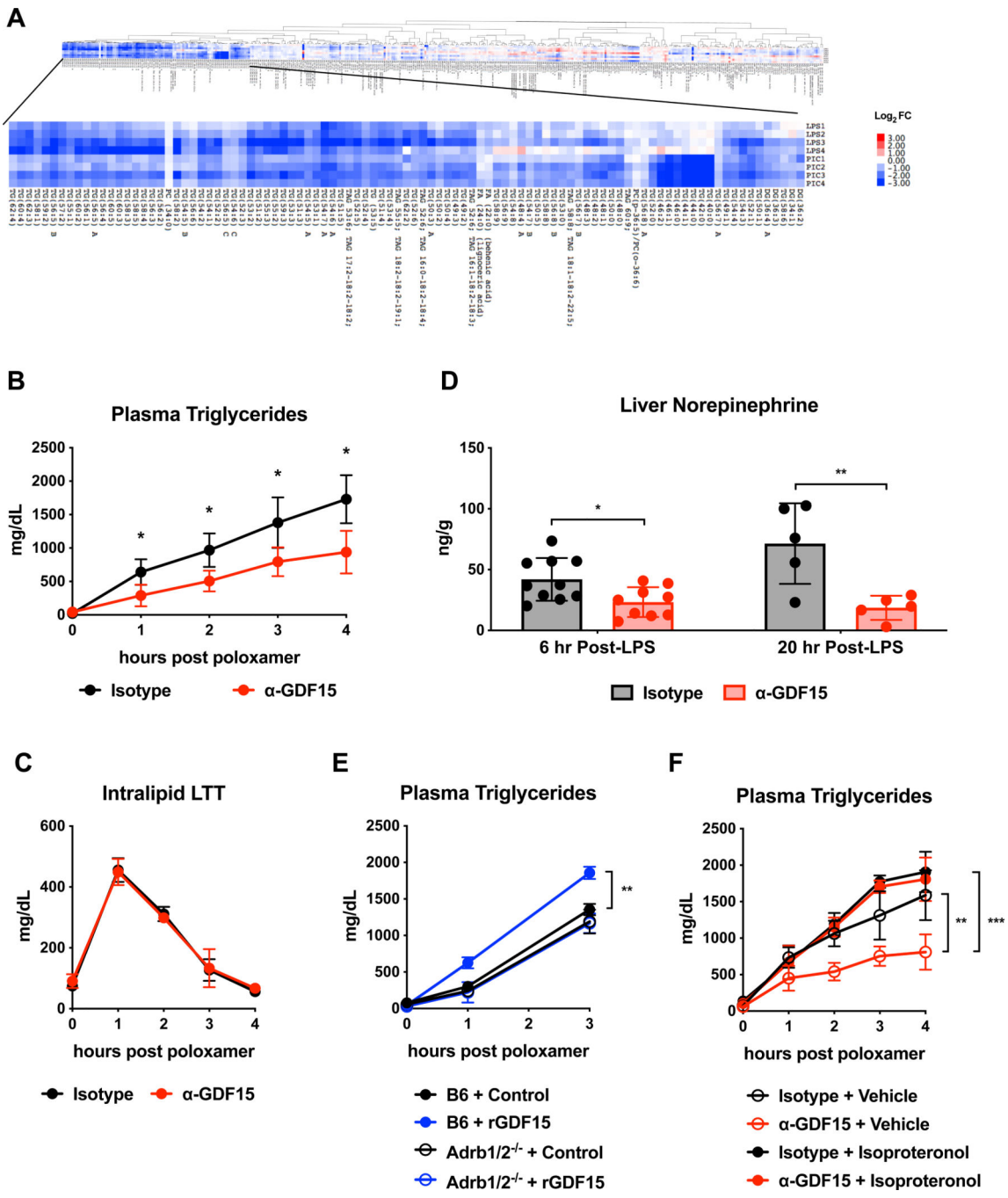

Figure 5. GDF15 controls triglyceride metabolism via hepatic adrenergic signaling.

(A) Lipidomics analysis from mouse plasma 12 hours after either LPS or Poly(I:C) injection following pre-treatment with either isotype or α-GDF15 antibody. Values are represented as log2 fold change of each α-GDF15 antibody pre-treated mouse over the average of all isotype mice in the respective group. DG=diacylglycerol, TG and TAG=triacylglycerol, PC=phosophocholine.

(B) Hepatic triglyceride export using the poloxamer method was measured in animals treated with isotype or α-GDF15 antibody at 24 hours after LPS challenge. (n=5 per group)

(C) An intravenous intralipid lipid tolerance test was performed in animals treated with isotype or α-GDF15 antibody at 24 hours after LPS challenge (n=5 per group)
(D) Norepinephrine levels in liver tissue 6 and 20 hours after LPS injection following pre-treatment with either isotype or α-GDF15 antibody.
(E) Hepatic triglyceride export using the poloxamer method was measured in wildtype and Adrb1/2$^{-/-}$ animals injected subcutaneously with rGDF15 30 minutes before poloxamer at 24 hours after LPS challenge. (n>4 per group, representative of 2 independent experiments using two different rGDF15 preparations)
(F) Hepatic triglyceride export using the poloxamer method was measured in animals treated with isotype or α-GDF15 antibody at 24 hours after LPS challenge with or without isoproterenol given at the time of poloxamer injection (n>8 per group).

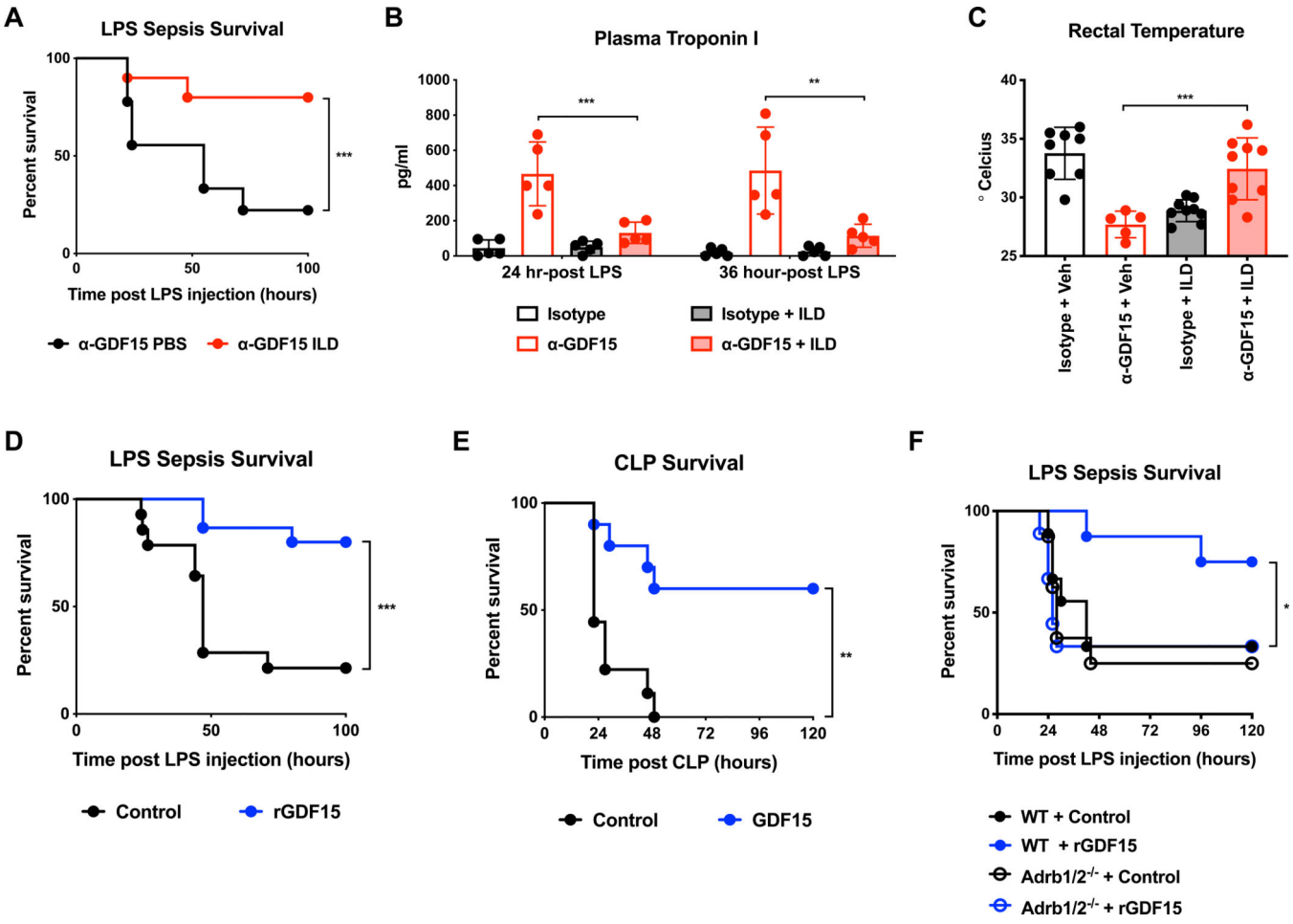

Figure 6. GDF15 controls triglyceride metabolism to support cardiac and thermal function during sepsis.

(A) Survival after intraperitoneal injection of LPS following pre-treatment with either isotype or α-GDF15 antibody and subsequent intraperitoneal injection of either PBS or Intralipid 20% at 2, 6, 22, and 30 hours post-LPS injection. (n>9 per group)

(B) Plasma troponin I levels 24 hours after LPS injection following pre-treatment with either isotype or α-GDF15 antibody with or without intraperitoneal injection of either PBS or Intralipid 20%.

(C) Rectal temperature in mice 24 hours after LPS injection following pre-treatment with either isotype or α-GDF15 antibody with or without intraperitoneal injection of either PBS or Intralipid 20%.

(D) Survival after intraperitoneal injection of LPS and subsequent injection of purified mouse GDF15 or control protein (ovalbumin) starting 6 hours post-LPS injection and twice daily thereafter. (n>14 per group, representative of 2 independent experiments using two different rGDF15 preparations)

(E) Survival after CLP and subsequent injection of purified mouse GDF15 or control protein (ovalbumin) starting 6 hours post-LPS injection and twice daily thereafter (n>9 per group).

(F) Survival in wildtype and Adrb1/2$^{-/-}$ animals after intraperitoneal injection of LPS and subsequent injection of purified mouse GDF15 or control protein (ovalbumin) starting 6 hours post-LPS injection and twice daily thereafter. (n>8 per group)

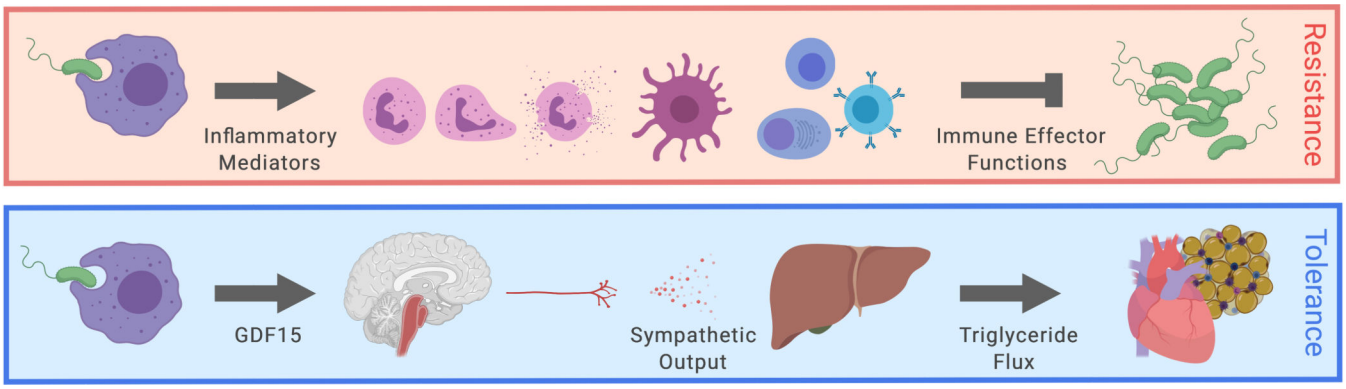

Figure 7. Model of GDF15 regulating hepatic sympathetic outflow controlling lipid metabolism to support cardiac function.

Upon inflammatory challenge, GDF15 is induced by immune and non-immune cells to control hepatic sympathetic outflow. Adrenergic signaling is required for maintaining systemic triglyceride levels necessary for supporting cardiac function during sepsis.

KEY RESOURCES TABLE

REAGENT or RESOURCE	SOURCE	IDENTIFIER
Antibodies		
Hamster monoclonal anti-TNF alpha (clone TN3–19.12)	eBioscience	Cat# 14–7423; RRID: AB_468492
Rat monoclonal anti-IL-6 (clone MP5–20F3)	eBioscience	Cat# 14–7061; RRID: AB_468423
Biotin-conjugated rabbit polyclonal anti-TNF alpha	eBioscience	Cat# 13–7341; RRID: AB_466951
Biotin-conjugated rat monoclonal anti-IL-6 (clone MP5–32C11)	BD	Cat# 554402; RRID: AB_395368
anti-cFos (Synaptic Systems,	Synaptic Systems	Cat# 226 003; RRID: AB_2231974
Donkey anti-Rabbit IgG (H+L) Highly Cross-Adsorbed Secondary Antibody, Alexa Fluor 647	Thermo Fisher Scientific	Cat# A-31573; RRID: AB_2536183
Rat Anti-IL-12 (p40 / p70) Monoclonal Antibody, Unconjugated (clone C15.6)	BD	Cat# 551219; RRID: AB_394097
Rat Anti-IL-12 (p40 / p70) Monoclonal Antibody, Biotin Conjugated (clone C17.8)	BD	Cat# 554476; RRID: AB_395419
Anti-mouse CD45-PE	eBioscience	Cat# 12–0451-81; RRID: AB_465668
Anti-mouse CD11b-APC	eBioscience	Cat# 17–0112-83; RRID: AB_469343
Anti-mouse F/480-AF488	Biolegend	Cat# 123120; RRID: AB_893479
Anti-mouse CD16/32 (clone 93)	eBioscience	Cat# 16–0161; RRID: AB_468900
Anti-mouse CD45-BUV395	eBioscience	Cat# 564279; RRID: AB_2651134
Anti-mouse Ly6G-FITC	Biolegend	Cat# 127606; RRID: AB_1236494
Anti-mouse CD8-PE	eBioscience	Cat# 553032; RRID: AB_394570
Anti-mouse CD3-PECy7	BioLegend	Cat# 100220; RRID: AB_1732057
Anti-mouse F/480-APC		Cat# 123116; RRID: AB_893481
Anti-mouse CD11b-Pacific Blue	eBioscience	Cat# RM2828, RRID: AB_10372795
Chemicals, Peptides, and Recombinant Proteins		
Intralipid 20%	Sigma-Aldrich	Cat# I141
Pluronic F-127	Sigma-Aldrich	Cat# P2443
Isoproteronol	Sigma-Aldrich	Cat# I-6504
2,3,7,8-Tetrachlorodibenzo-p-dioxin	Sigma-Aldrich	Cat# 48599
Lithium chloride	Sigma-Aldrich	Cat# L4408
Lipopolysaccharide from *E. coli* strain 055:B5	Sigma-Aldrich	Cat# L2880
Poly(I:C)	Invivogen	Cat# tlrl-pic-5
Collagenase IV	Worthington Biochemical Corporation	Cat# LS004189
Collagenase II	Worthington Biochemical Corporation	Cat# LS004174
Collagenase/Dispase Solution	Roche	Cat# 10 269 638 001
2DG	Sigma-Aldrich	Cat# D6134
AICAR	Tocris	Cat# 2840
R837	Invivogen	Cat# tlrl-imq
RNA-Bee	Tel Test, Inc	Cat# CS-501B

REAGENT or RESOURCE	SOURCE	IDENTIFIER
SMART MMLV Reverse Transcriptase	Clontech	Cat# 639524
Low ROX PerfeCTa SYBR Green SuperMix	Quanta	Cat# 95056
Ethidium monoazide bromide	Biotium	Cat# 40015
Critical Commercial Assays		
Mouse IFNα ELISA kit	ThermoFisher Scientific	Cat# BMS6027
Mouse Cardiac Troponin-I ELISA kit	Life Diagnostics	Cat# CTNI-1-HSP
Alanine Transaminase Activity Assay Kit	Cayman Chemical	Cat# 700260
Non-esterified Fatty Acid Assay Reagent	Wako Diagnostics	Cat# 999–34691, Cat# 995–34791, Cat# 991–34891, Cat# 993–35191
β-hydroxybutyrate Assay Kit	Cayman Chemical	Cat# 700190
RNeasy Mini Kit	Qiagen	Cat# 74106
Norepinephrine	Eagle Biosciences	Cat# NOR31-K01
Amylase	Abcam	Cat# 102523
Qiagen's DNeasy UltraClean Microbial Kit	Qiagen	Cat# 12224–50
Experimental Models: Organisms/Strains		
Mouse: C57BL/6J	The Jackson Laboratory	Stock No. 000664
Mouse: *Adrb1*^{tm1Bkk} *Adrb2*^{tm1Bkk}/J	The Jackson Laboratory	Stock No. 003810
Influenza: Strain A/WSN/33	Akiko Iwasaki (Lund et al., 2004)	
Sequence-based Reagents		
Supplemental Table S3	This paper	
Software and Algorithms		
Imaris software	Bitplane	
Visual Sonics Vevo 2100	Fujifilm	
Other		
4–0 silk	Ethicon	Cat# A184
4–0 chromic gut	CP Medical	Cat# 121CG
Rectal probe thermometer	Physitemp	TH-5 Thermalert
Lysing Matrix D, 2 mL Tube	MP Biomedicals	Cat# 116913500
Plasma separator tubes	BD	Cat# 365985